# Towards Automated BIM and BEM Model Generation using a B-Rep-based Method with Topological Map

Oscar Roman[1,2], Gabriele Mazzacca[1,3], Elisa Mariarosaria Farella[1], Fabio Remondino[1], Maarten Bassier[4], Giorgio Agugiaro[5]

[1] 3D Optical Metrology (3DOM) unit, Bruno Kessler Foundation (FBK), Trento, Italy
Email: {oroman, gmazzacca, elifarella, remondino}@fbk.eu

[2] Department Information Engineering and Computer Science (IECS), University of Trento, Trento, Italy - oscar.roman@unitn.it

[3] Department of Mathematics, Computer Science and Physics, University of Udine, Italy - mazzacca.gabriele@spes.uniud.it

[4] Department of Civil Engineering, TC Construction – Geomatics, KU Leuven - Faculty of Engineering Technology Ghent, Belgium
maarten.bassier@kuleuven.be

[5] School of Architecture and Built Environment, Delft University of Technology, the Netherlands - g.agugiaro@tudelft.nl

**Keywords:** Automation in construction, BIM, BEM, B-Rep method, Computational Geometry, Digital Twin

**Abstract**

In many countries, recent boosts in the construction and renovation sectors and energy efficiency directives are driving a growing interest in the built environment among designers and maintainers. In this context, customized software solutions tailored for Building Information Modelling (BIM) and Building Energy Modelling (BEM) are proving to be indispensable for optimizing operational efficiency within the Architecture, Engineering, Construction, Owner, and Operator (AECOO) sector and for facilitating the generation of buildings' Digital Twins (DTs). These DTs rely on accurate geometry and ancillary information (semantics, sensors, etc.) to define properties of single elements, enabling crucial simulations in structural conditions or energy needs. However, BIM and BEM model creation and their enrichment with semantic information are highly time-consuming and prone to manual errors. Hence, there is an increasing demand for automatic methods featuring a high level of geometric accuracy to reconstruct building elements, such as walls, floors, and openings captured via 3D reality-based surveying. This paper introduces an automated method for creating Boundary Representation (B-Rep) models from 3D surveying data for the generation of digital building replicas. The method is based on the detection and computation of topological elements from 3D reality-based point clouds. It proves valuable for architectural or design workflows and for conducting energy or quality system simulations.

## 1. Introduction

The concepts of Building Information Modelling (BIM), Building Energy Modelling (BEM) and Digital Twin (DT) are rapidly modifying conventional approaches to manage the design/construction (Bassier et al., 2020a; Olimat et al., 2023) and the monitoring/maintenance (Cao et al., 2022; Sampaio et al., 2021; Zhou et al., 2023) phases for civil and industrial structures (Nguyen and Adhikari, 2023). DTs from BIM and BEM models are increasingly requested for building renovations (Doukari et al., 2024), for monitoring the behaviour of infrastructures (Ahmad et al., 2024) and for improving energy efficiency (Yang et al., 2022; Chen et al., 2024). Therefore, it is crucial to advance the BIM/BEM generation process, targeting faster and more automated methods that rely on accurate data to support the modelling phase. Reality-based 3D surveying techniques, such as LiDAR or photogrammetry or their simultaneous usage (Yang et al., 2023), are mature enough to ensure highly accurate 3D point clouds or meshes also in large-scale mapping projects (Kang, 2023). However, for structural or energy analyses, it is crucial that models consist of a limited yet precise set of elements, such as slabs, walls, and openings, ensuring seamless interoperability without any loss of data, typically facilitated through standardized formats like Industry Foundation Class (IFC) and Green Building XML (gbXML) (Yang et al., 2022).

The paper introduces an innovative Boundary Representation (B-Rep) method for reconstructing some architectural elements from point clouds and increasing automation in the realization of BIM/BEM products. The method starts from unstructured point clouds and follows various automated steps. The B-Rep method is used to represent solid objects and surfaces through their boundaries, such as vertices and edges, and the rules of computational geometry define the relationship among elements. While the B-Rep geometrical model is generally not used to represent objects in a BIM model (a CSG is commonly preferred instead), the geometries produced with the proposed method are nonetheless compatible with BIM/BEM environments, enabling their utilization in various applications.

### 1.1 Aim and contribution of the work

The proposed B-Rep based method for reconstructing solid objects and surfaces in BIM and BEM applications offers a comprehensive geometric approach to extract topological elements like vertices and edges, constructing a *Topological Map*. This map uses line intersections and directional vectors to reconstruct objects and surfaces, enabling independent computation of BIM and BEM models without data loss. Experiments and analyses, leveraging different datasets and comparing solid-based and surface-based models with respect to Ground Truth (GT) data, showcase the valuable contribution of the proposed procedure.

## 2. State of the art

In recent years, advancements in Machine Learning (ML) (Xu and Stilla, 2021) and Deep Learning (DL) techniques (Charles R. Qi et al., 2017) have yielded significant improvement in the classification of structural elements within buildings, while semi-automatic reconstructions of BIM/BEM objects from classified data and structured point clouds is still a challenge (Roman et al., 2023a; Roman et al., 2023b). Parametric modelling, such as model matching or fitting, based on geometric shapes and

mathematical expressions, could be used for reconstructing building elements from structured point clouds through primitive geometries and masses, and also their mechanical, electrical and plumbing (MEP) systems (Lee et al., 2023).

Benchmarks (Khoshelham et al., 2020) based on shared and synthetic datasets have been created to compare the performance of various automatic BIM reconstruction methodologies (Bassier et al., 2020b; Tran and Khoshelham, 2020; Ochmann et al., 2019; Maset et al., 2019), thereby enabling the assessment of developed models for future advancement.

Typically, Scan-to-BIM processes implemented in the different methods prioritize a limited number of element classes, as shown in Table 1.

| Method | Windows | Doors | Pillars | Walls | Floors |
|---|---|---|---|---|---|
| Yang et al. 2023 | ✗ | ✗ | ✗ | ✓ | ✗ |
| Tran and Khoshelham, 2020 | ✗ | ✗ | ✓ | ✓ | ✓ |
| Liu et el., 2022 | ✗ | ✓ | ✗ | ✓ | ✓ |
| Bassier et a., 2020 | ✗ | ✗ | ✓ | ✓ | ✓ |
| Ochmann et al., 2019 | ✗ | ✗ | ✗ | ✓ | ✓ |

Table 1. Some of the developed Scan-to-BIM methods targeted on the reconstruction of selected architectural elements.

In recent years, B-Rep based methods have been re-evaluated for their efficiency in various applications (Hou et al., 2023), such as the extraction of contours and edges of indoor spaces from point cloud data, as demonstrated by Ahmed et al. (2018) and Schmidt et al. (2023).

Furthermore, some latest approaches (Lee et al., 2023) tend towards the integration between structural elements of the buildings, like columns, walls and slabs (Yang et al., 2023), and openings, both on the facades (Wysocki et al., 2023; Ning et al., 2021), and in indoor environments (Liu et el., 2022).

## 3. Method

The proposed method through different operations and pipelines, the method (Figure 1) enables the automatic reconstruction of walls, slabs, and windows from semantically enriched point clouds based on the detection and computation of geometric primitives and topological elements. Geometric primitives, such as points and lines used for building plan representation, are automatically extracted from unstructured point cloud data, defined solely by coordinates $\mathcal{C}$.

### 3.1 The reconstruction workflow

In the proposed method (Figure 1), two parallel processes enable the reconstruction of some structural elements, while a specific pipeline is implemented for windows. The different workflows share the pre-processing phase, which includes the classification of building elements.

For walls and slabs reconstruction, the workflow includes:
1. **Plane detection** with RANSAC algorithm, based on CGAL (Hemmer, M., 2024) algorithm to extract the main geometric primitives.
2. **Line extraction and generation of the *Topological Map*:** lines are extracted from the point cloud to generate the *Topological Map* (Section 3.2). From this map, it is possible to generate walls and, by utilizing the perimeter segments, create slabs.

For windows reconstruction, the pipeline involves:

1. **DBSCAN** (Hahsler and Piekenbrock, 2023) algorithm to cluster individual windows (instance segmentation);
2. **Principal Component Analysis (PCA)** used to compute their dimension and position.

Finally, all the elements are automatically reconstructed, generating both solid and surface-based models.

The following section reports more insight into the *Topological Map* creation for generating the final BIM/BEM models. Some examples of the generated outputs are provided in Section 4.
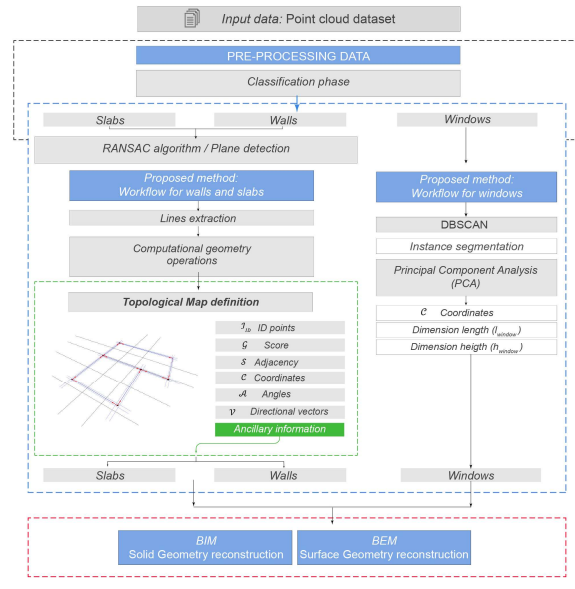


Figure 1. The proposed workflow for the BIM and BEM 3D data generation.

### 3.2 The Topological Map

The *Topological Map* (Figure 2) is the key representation used in this work for the reconstruction of primary elements, like walls and slabs, obtained through a series of computational geometric operations. Each algorithm computes and operates with arrays or tensors to store information for the creation of the *Topological Map*, which is the final 2D vector restitution of the building floor plan.

Similar to an oriented graph (Jiang et al., 2023), the Topological Map assigns a weight ($\mathcal{G}$) to the vertices and a direction ($\mathcal{V}$) to the links, and it mainly consists of:
- *Intersection Key points* (nodes), with coordinates $\mathcal{C}$, score $\mathcal{G}$, and Identification number $\mathcal{I}_{ID}$. The *score* $\mathcal{G}$ is determined by the number of intersecting lines converging at each point.
- *Segment lines* (edges), which link each corresponding intersection point $\mathcal{I}_i$ through directional vectors.
- *Directional vectors*, featured by *angles* $\mathcal{A}$ and *vectors* $\mathcal{V}$.

The extraction of geometric information occurs through several steps:
1. **Lines extraction:** from the planes extracted by RANSAC algorithm (Section 3.1), users can define a section plane $\pi_{sec}$, which can be customized with a specific height along the local z-axis and a buffering area $\eta$ (Figure 3.a);
2. **Outlier removal and merging:** the algorithm filters out extracted lines shorter than predefined thresholds *(Δl)*. Then, it assesses the directional vector of nearby lines, evaluates the angle between them, and merges collinear lines if the angle is below a specified threshold *(Δα)* (Roman et al., 2023b);

3. **Line extension:** detected lines are extended along the direction vectors to compute all the intersection points ($\mathcal{I}$). Lines are extended until the first intersection point and, additionally, up to a pre-set limit around the point cloud. Then, if two points $\mathcal{I}$ are close to each other and their vectors are parallel, their coordinates are normalized along the main direction of the lines, in order to facilitate the search for lines to pair in the subsequent phase;

4. **Pairing lines:** pairs of parallel lines, representing both the internal and external surfaces of walls, are formed by evaluating the proximity between vertices of lines while also assessing the parallelism between them. Furthermore, the algorithm computes and stores the Euclidean distance between paired lines, which correspond to the wall thickness *(th_wall)* (Section 3.3);

5. **Computation of the centre lines:** from couples of paired lines, the algorithm computes the central lines, i.e., the equidistant lines between them;

6. **Computation of Intersection Key points:** they represent the vertices defining the spatial layout to be reconstructed. Together with directional vectors, they are the fundamental elements for reconstructing the *Topological Map* of the building plan (Figure 3).
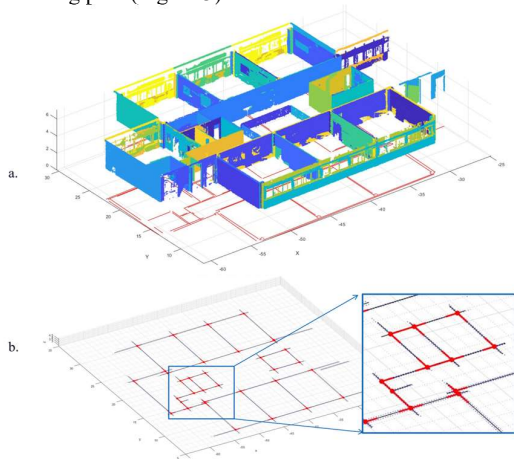


Figure 2. Definition of the *Topological Map*: a) lines extraction from a point cloud; b) the *Topological Map* with Intersection Key points $\mathcal{I}$ (red points) and directional vectors $\mathcal{V}$ (red arrows).

At this point, the Adjacency Matrix $\mathcal{S}$ is computed. It links the $\mathcal{I}_{ID}$ of the i-*th* points, which are connected among them by a vector (Equation 1):

$$\mathcal{S} = \mathcal{I} \bullet \mathcal{G} = \begin{bmatrix} i_{1,1} & \cdots & i_{1,n} \\ \vdots & \ddots & \vdots \\ i_{n,1} & \cdots & i_{n,n} \end{bmatrix} \begin{bmatrix} g_{1,1} & \cdots & g_{1,n} \\ \vdots & \ddots & \vdots \\ g_{n,1} & \cdots & g_{n,n} \end{bmatrix} \quad (1)$$

This method allows for accessing information about the same $\mathcal{I}$ point in each array and, therefore, anchors and associates Intersection Key Points ($\mathcal{I}$) and directional vectors ($\mathcal{V}$) within the *Topological Map*. This map, which enables the building plan reconstruction, is defined as (Equation 2):

$$\mathcal{L} = Topological\ Map = \mathcal{I} \bullet \mathcal{G} \times \mathcal{V} = \mathcal{S} \times \mathcal{V} \quad (2)$$

Where $\mathcal{V} = [\mathcal{V}_1, \dots, \mathcal{V}_n]$ is a tensor and each vector is defined as $\mathcal{V}_i = [v_1, \dots, v_k]$ with $k \in \mathbb{R}$ such that $1 \le k \le 4$. Here $k$ represents the four possible directions around a point, characterized by angles stored in the $\mathcal{A}$ array.

### 3.3 Reconstruction method

The *Topological Map* serves as a base for both solid and surface reconstructions of walls and slabs, while a different workflow, as anticipated in Section 3.1, is employed for the reconstruction of secondary elements, in particular, windows (Figure 1).
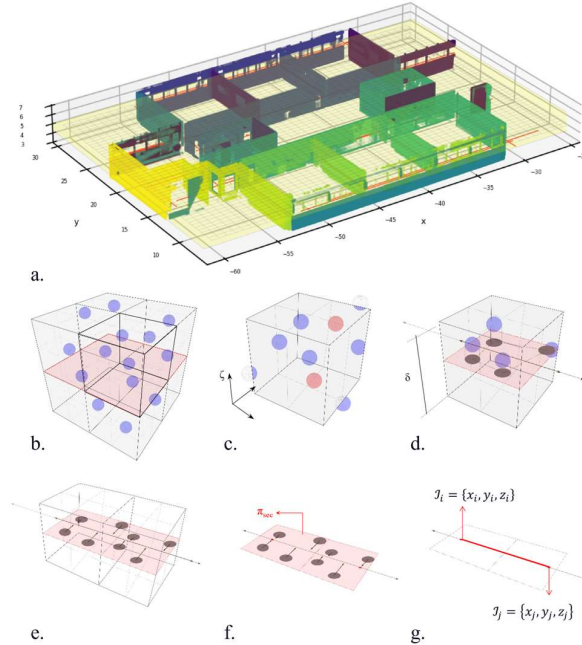


Figure 3. In the upper figure: a) the section plane $\pi_{sec}$ (yellow plane) cutting the RANSAC-extracted planes. In the lower figures, a graphic representation of the lines extraction: b) buffer area *(η)* above and below the section plane c) points down sampling; d) and e) projection of collected points onto the section plane *(π_sec)*; f) application of PCA; g) definition of the extreme points and tracing of the segment lines.

**3.3.1 Walls reconstruction:** Wall surfaces are planar objects that can be described by two points, featured by their *(x, y, z)* coordinates and their height (*h*) along the *z* axis. B-Rep methods use topological objects, such as vertices and edges, to geometrically describe them.

In our method, in the case of structural elements, once generated the *Topological Map*, the directional vectors ($\mathcal{V}$) are used as guides for connecting segments between Intersecting Points ($\mathcal{I}$). Subsequently, walls are anchored and reconstructed along the segments using their centreline and the corresponding length *(l_ij)*. While the wall thickness is derived from the operation of pairing lines (Section 3.2), the height is automatically computed from the classified point cloud and assigned to the generated models. After filtering noisy points, the coordinates of the highest ($z\_max$) and the lower ($z\_min$) points within the walls class are used to define levels within the model.

**3.3.2 Slabs reconstruction:** Slabs, instead, are reconstructed from the centre lines of the external segments delineating the perimeter of the floor plan. The reconstruction of the slabs typically involves delineating the boundary lines to define the floor's perimeter on the plan view. The algorithm, as for the wall reconstructions, uses Intersection Key Points ($\mathcal{I}$) and retrieves the Directional Vector ($\mathcal{V}$) to close the polygon following a counterclockwise direction. Slabs height is automatically derived from the correspondent classified point cloud, similar to the wall case. The algorithm, in fact, uses the points with the highest

($z\_max$) and the lower ($z\_min$) $z$ coordinates within the floor class to define the slab thickness (noise is filtered out before running this operation).
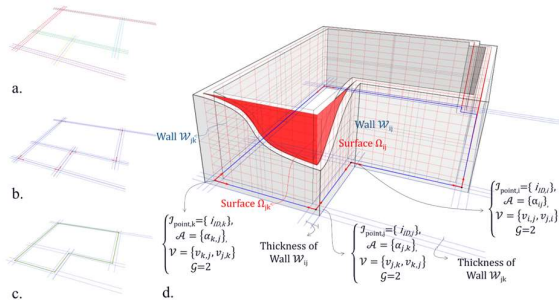


Figure 4. The *Topological Map* generation: a) pairing lines; b) intersection points and directional vectors; c) segment lines; d) the *Topological Map,* useful for solid and surface-based models, composed of Intersection Key Points ($\mathcal{I}$), Score Array ($\mathcal{G}$), Angles ($\mathcal{A}$) and Vectors ($\mathcal{V}$) to define Surfaces ($\Omega$) and Walls ($\mathcal{W}$).

In this way, both solid walls and slabs for BIM applications and surface-model are derived from the same input data (Figure 4). In the surface-based model, external walls are delineated by their external lines, while internal walls and partitions are reconstructed using centre lines, in accordance with standard conventions (Yang et al., 2022).

**3.3.3 Windows reconstruction:** Openings are also significant elements in defining the energy class of the building. In fact, when considering energy efficiency, the critical aspect of openings lies in their glass area, which determines the heat flux through the structure.

The workflow for the windows restitution consists of (Figure 15):
• windows class extraction from the classified point cloud;
• use of the DBSCAN algorithm along with normals $n_x$, $n_y$, for an efficient instance segmentation;
• apply a Principal Component Analysis (PCA) to each cluster, computing the length of the cluster ($l$) and height($h$);
• transfer cluster length and height information and the relative coordinates ($x_{loc}$, $y_{loc}$, $z_{loc}$) inside the BIM and BEM environments for the reconstruction and correct positioning of the elements.

This information guides the automatic placing of pre-built and external windows components within the model. In the current implementation, the pre-built window element is a generic and single-frame component, that automatically adapts to the dimensions of detected openings (Section 4.3.3).

## 4. Experiments and results

### 4.1 Datasets

In order to test the capability, reliability, and limitations of the implemented reconstruction method, different LiDAR-based datasets are leveraged for the experiments (Table 2) (Figure 5). While Building01 is a dataset coming from a collaborating company, Building02 (TUB1) and 03 (TUB2) derive from an ISPRS benchmark (Khoshelham et al., 2020).

Point cloud datasets used for the reconstruction are also used as ground truth (GT) in the metric assessment of solid-based reconstructed models (BIM). For the energy model (BEM), a surface ground truth is manually modelled, following the single energy border standard assumption without gaps (Yang et al., 2022) (Section 4.4).
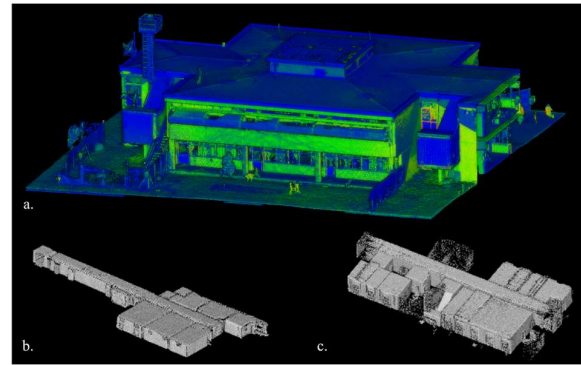


Figure 5. The testing datasets: a) Building01, school building; b) Building02 and c) Building03 (Khoshelham et al., 2020).

| # Dataset | # Level | Num. of points [*mill.*] | Average Distance [*mm*] | RGB |
|---|---|---|---|---|
| *Building01* | *First floor* | 27.79 | 5 | ✓ |
| *Building02 (TUB1)* | *Gr. Floor* | 33.60 | 5 | ✗ |
| *Building03 (TUB2)* | *First floor* | 21.60 | 8 | ✗ |

Table 2. Characteristics of the datasets used in the reconstruction experiments.

### 4.2 Data pre-processing

***Point cloud classification:*** both a Machine Learning (Random Forest) (Grilli and Remondino, 2020) and an in-house DL approach based on Point Transformer (Zhao et al., 2021) are tested in the experiments. As the focus of the reconstruction is on walls, slabs, and windows (Figure 6), the models are fine-tuned to map the abovementioned classes.
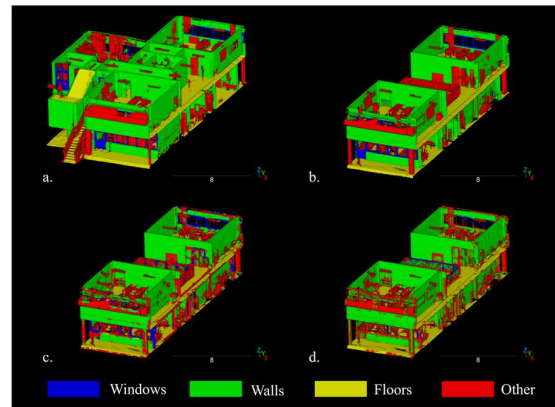


Figure 6. Classification results for the Bulding01 dataset: a) Training set; b) Manually labelled evaluation set (GT); c) Point Transformer prediction on the evaluation set; d) Random Forest prediction on the evaluation set.

While the outcomes of both methods are comparable, the DL method performs marginally better, particularly when it comes to the Recall statistic, and it has been selected for the reconstruction phase. It is likely that the DL results could significantly improve with more training data. Furthermore, additional studies are needed to determine the degree to which these models can be

generalizable. Example results of the classification for the Building01 dataset are reported in Table 3.

| Building01 | | | |
|---|---|---|---|
| **Deep Learning – Point Transformer** | | | |
| **Class** | **Precision** | **Recall** | **F1-Score** |
| Windows | 0.59 | 0.61 | 0.60 |
| Walls | 0.85 | 0.86 | 0.85 |
| Floors | 0.96 | 0.95 | 0.96 |
| Other | 0.66 | 0.66 | 0.66 |
| **Machine Learning – Random Forest** | | | |
| **Class** | **Precision** | **Recall** | **F1-Score** |
| Windows | 0.70 | 0.23 | 0.35 |
| Walls | 0.80 | 0.87 | 0.83 |
| Floors | 0.95 | 0.97 | 0.96 |
| Other | 0.61 | 0.59 | 0.60 |

Table 3. Metrics of the classification ML and DL approaches for the Building01 dataset, calculated on the evaluation set prediction.

**Planes Extraction:** Starting from classified point clouds, a RANSAC algorithm is employed for the wall class. The parameters of the RANSAC algorithm are fine-tuned to extract planar surfaces from classified wall elements within the point cloud (Figure 7).
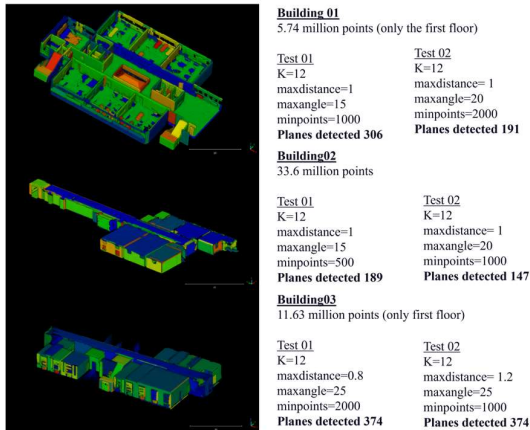


Figure 7. Some results of the CGAL-based plane detection on Building01, Building02 (TUB 1), and Building03 (TUB 2) datasets.

## 4.3 BIM and BEM reconstruction

**Lines extraction:** On vertical RANSAC-detected planes, a horizontal section plane ($\pi_{sec}$) is generated to enable the lines extraction (Section 3.2). The height of the $\pi_{sec}$ plane is defined by the user and should be set by preferring areas with higher completeness and density of points (Figure 8). A vertical buffer ($\eta$) can be included to minimize errors by gathering additional points along the vertical axis. Lines are then defined as intersections between the vertical planes of the walls and the generated $\pi_{sec}$ plane. Figure 8 illustrates different outputs by varying the section height.

**Computational geometry application:** once extracted lines, a series of geometric operations are applied (Section 3.2) to compute the *Topological Map*, in order to define the number of Intersection Key Points ($\mathcal{J}$), and the type of connections between walls through the Adjacency Matrix $\mathcal{S}$.
Reconstruction of slabs are obtained from the centre lines of the external segments delineating the perimeter of the floor plan and it is also applicable to multi-floor buildings (Figure 9).
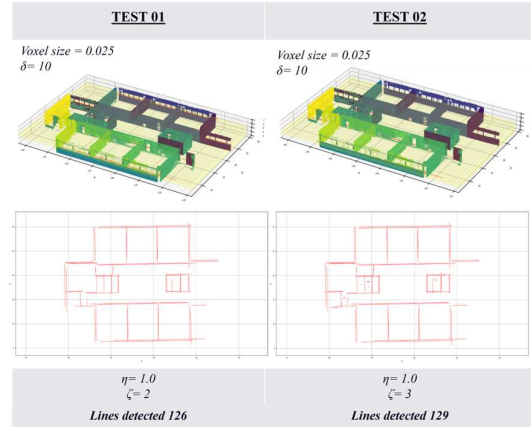


Figure 8. Examples which illustrate the extraction of lines varying the section heights ($\zeta$) and vertical buffer sizes ($\eta$).
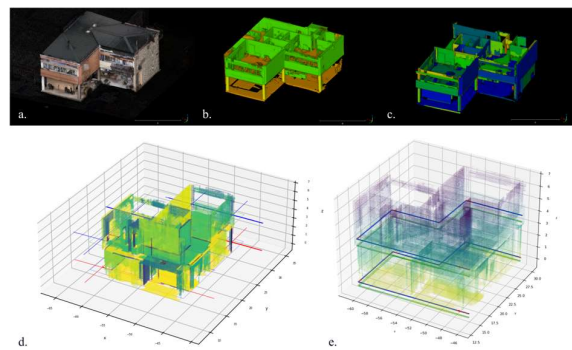


Figure 9. Phases of the slabs extraction (portion of Building 01): a) the input point cloud; b) semantic segmentation of structural elements; c) planes detected through RANSAC; d) lines extraction for different floors; e) the *Topological Map* definition and slabs computation.

### 4.3.1 Primary elements: walls

Some results of the reconstruction phase, both for solid and surface-based models, on the testing datasets are presented in Figure 10.
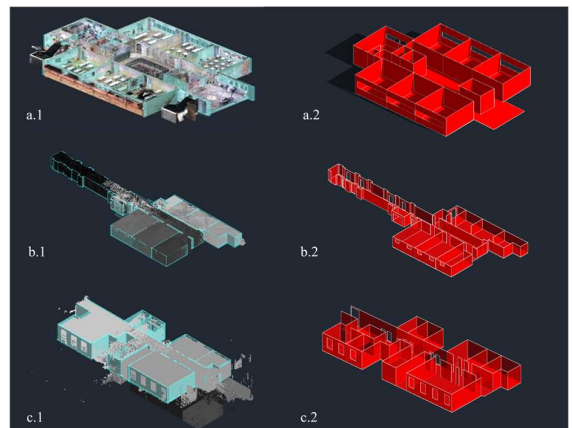


Figure 10. Reconstruction of elements for the three datasets. On the left, the solid models (blue elements, visualized with the input point clouds); on the right, the generated surface models.
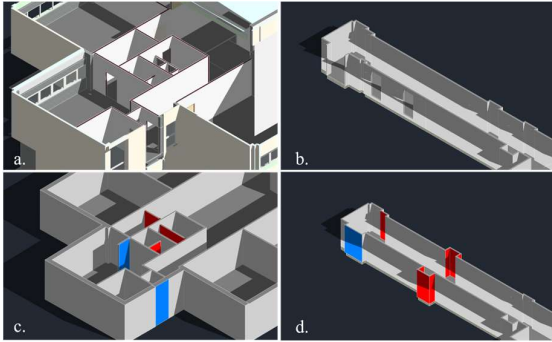
Figure 11. The results of the reconstruction method. a) and b) the GT IFC model for Building01 and Building02; c) and d) some errors in the elements' reconstruction.

Since the thickness and the height of the walls are defined through ancillary information extracted from the input data (Section 3.3), the reconstruction results are deeply impacted both by the accuracy of classification and by the line extraction phase. A visual assessment of the obtained models is shown in Figure 11, highlighting some inaccuracies in the wall's reconstruction. It includes deficiencies in dimensions (red colour), incorrect positioning of the element, and reconstruction errors occurring in data-deficient regions (blue colour).

Figure 12 illustrates additional reconstruction errors, specifically showcasing inaccurately identified walls pertaining to distinct architectural elements like indentations within the structure.
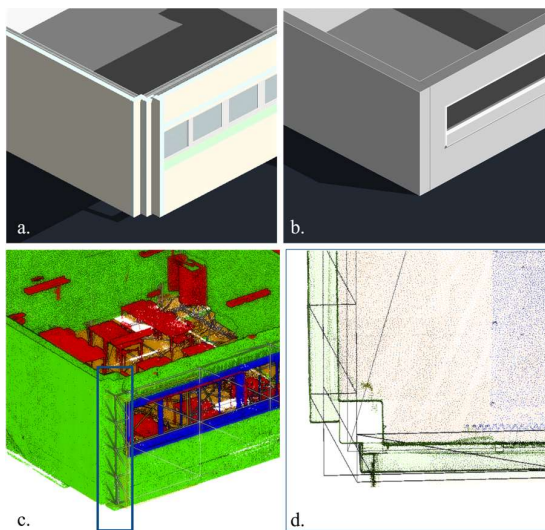


Figure 12. Some issues in the reconstruction of Building01. a) the ground truth BIM model; b) the reconstructed model; c) and d) the point cloud and the solid model overlapped, highlighting the error in a 3D and plan view (in green, the point cloud of the envelope; in white, the solid model reconstruction with a simplified orthogonal intersection).

### 4.3.2 Primary elements: slabs

Figure 13 presents some results on a section of the first floor of Building01, while Figure 14 shows the reconstructed slab from the *Topological Map*.

This approach could fail in extracting balconies and further ledges since the line's extraction is based on external walls, and railings could not be detected.
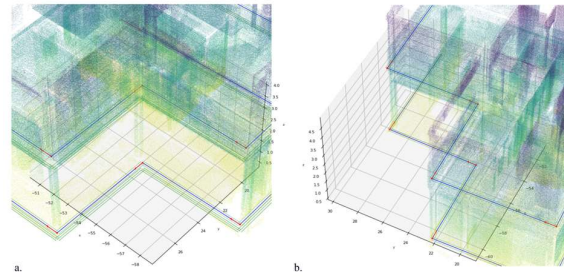


Figure 13. A zoomed view on the *Topological Map* for floor restitution: a) south-east view and b) north-east view.
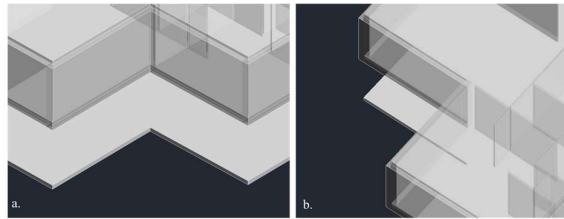


Figure 14. Some views of the slabs reconstructed for the BIM model.

### 4.3.3 Secondary elements

Regarding windows, a DBSCAN algorithm for instance segmentation is applied to cluster elements, and a PCA is performed to compute the dimensions of each detected window and their positioning within the models.

Some example results of the automatic windows reconstruction are shown in Figure 15. As anticipated in Section 3.3, a pre-built component (the the blue single-frame object visible in the figure) is automatically placed and adapted to cover the surface detected and classified as an opening in the input point cloud.
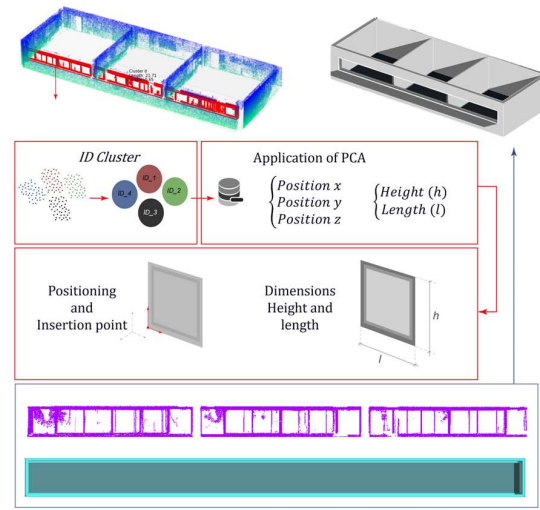


Figure 15. Windows reconstruction workflow and results on a section of Building 01 dataset.

### 4.4 Assessment of the BIM and BEM derived models

Once the solid and surface models are obtained, a geometric assessment have been performed to assess the validity of the presented method.

Assuming the input point cloud as GT for the BIM and the manual surface model for the BEM, metric and visual results are reported in Table 4 and Figures 16 and 17.

| Building | Average distance (signed) [m] | Standard Deviation (signed) [m] | Max Error [m] |
|---|---|---|---|
| Building01_Solid | 0.062 | 0.076 | 0.138 |
| Building01_Surface | 0.017 | 0.082 | 0.099 |
| Building02_(TUB1) Solid | 0.053 | 0.108 | 0.162 |
| Building02 (TUB1) Surface | 0.021 | 0.092 | 0.113 |
| Building03 (TUB2) Solid | 0.094 | 0.112 | 0.205 |
| Building03 (TUB2) Surface | 0.023 | 0.092 | 0.115 |

Table 4. Metric assessment for the solid (BIM) and the surface (BEM) reconstructed models (Cloud-to-Mesh).

The solid model of Building03, which exhibits more complex geometry, demonstrates the poorest metrics, with a deviation of approximately 11 cm from the reference model. The building presents a high thickness of some walls and significant number of internal doors, resulting in reduced accuracy of the reconstructed walls compared to the GT. Conversely, the surface-based model shows slightly higher accuracy as both the reconstructed surface and the GT solely reference the central and perimetral lines, thus minimizing errors.

Overall, the high value of the standard deviation can be attributed to noise points within the input point clouds (GT), along with indoor doors not being reconstructed and some issues with fine-tuning the correct height of the floor slabs.
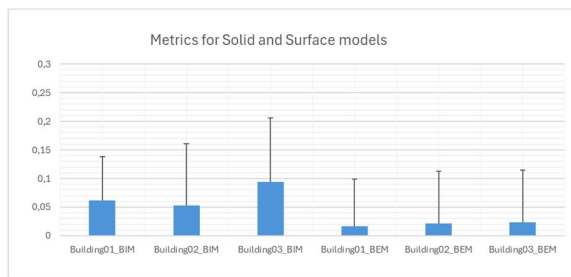


Figure 16. Metric assessments for the solid and the surface models (average and standard deviation) (Cloud-to-Mesh).

## 5. Conclusions and future works

The paper proposed an automated method for deriving solid and surface models from pre-classified point clouds. Once the *Topological Map* and its features are defined for walls and slab reconstruction, solid objects and surfaces can be directly derived for further uses in BIM and BEM environments. A further pipeline is proposed for the automatic reconstruction of windows. Moreover, this method facilitates the autonomous generation of the two models, significantly reducing data loss and fostering interoperability among different platforms and environments without being reliant on external sources for model derivation.

The presented experiments highlight the potential of the method in boosting automation in BIM and BEM modelling applications, as well as some limitations of the current implementation.

The quality and accuracy of reconstruction are significantly influenced by the noise level in the input point cloud, especially during line extraction, a critical phase in the pipeline. Experiments has highlighted challenges in reconstructing walls, particularly with features like indentations and balconies. Fine-tuning the slab extraction pipeline could address these issues by extracting edges from point cloud features. Improving window classification accuracy is crucial for their positioning and dimensions; this could be achieved with more training data.
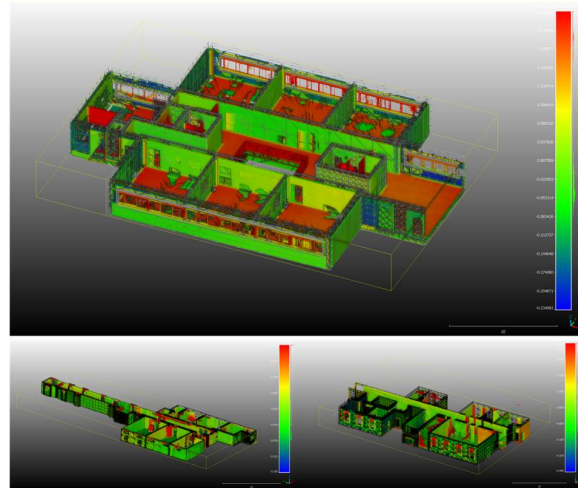


Figure 17. Example of Cloud-to-Mesh results (BIM solid models).

Expanding classification to include more elements like pillars and doors could enhance modelling for energy analysis, as well as systems and facilities (e.g., lights, radiators), but the effectiveness of automatic detection and modelling of these elements relies on a previous accurate point cloud classification. This approach ensures that the resulting BIM model is enriched with essential energy-related information, encompassing climate data and energy requirements. By exporting models in gbXML format, the link between Building Energy Modelling (BEM) and Digital Twin environments is enhanced. Associating energy-related information with reconstructed geometric elements further strengthens this connection, facilitating real-time data utilization for simulation, management, or visualization, and aiding in making decisions on energy efficiency and performance optimization.

## References

Ahmad, D.M., Gáspár, L., Bencze, Z. and Maya, R.A., 2024. The Role of BIM in Managing Risks in Sustainability of Bridge Projects: A Systematic Review with Meta-Analysis. *Sustainability*, 16(3), 1242.

Ahmed, S.M., Tan, Y.Z., Chew, C.M., Al Mamun, A., Wong, F.S., 2018. Edge and corner detection for unorganized 3d point clouds with application to robotic welding. *IEEE/RSJ International Conference on Intelligent Robots and Systems*, pp. 7350-7355.

Bassier, M. and Vergauwen, M., 2020a. Topology reconstruction of BIM wall objects from point cloud data. *Remote Sensing*, 12(11), 1800.

Bassier, M., Vincke, S., De Winter, H., Vergauwen, M., 2020b. Drift Invariant Metric Quality Control of Construction Sites Using BIM and Point Cloud Data. *ISPRS Int. J. Geo-Inf.*, 9(9), 545.

Cao, Y., Kamaruzzaman, S.N., Aziz, N.M., 2022. Building Information Modeling (BIM) Capabilities in the Operation and Maintenance Phase of Green Buildings: A Systematic Review. *Buildings*, 12(6):830.

Charles, R. Qi, Yi, L., Hao, S., Guibas, L. J., 2017. PointNet: Deep Learning on Point Sets for 3D Classification and Segmentation. *Computer Vision and Pattern Recognition (CVPR)*.

Chen, Z., Chen, L., Zhou, X., Huang, L., Sandanayake, M., Yap, P.S., 2024. Recent Technological Advancements in BIM and LCA Integration for Sustainable Construction: A Review. *Sustainability*, 16(3), 1340.

Doukari, O., Wakefield, J., Martinez, P. and Kassem, M., 2024. An ontology-based tool for safety management in building renovation projects. *Journal of Building Engineering*, 84.

Grilli, E., Remondino, F., 2020.Machine Learning Generalisation across Different 3D Architectural Heritage. *ISPRS International Journal of Geo-Information*, 9(6):379.

Hahsler, M., Piekenbrock, M., 2023. dbscan: Density-Based Spatial Clustering of Applications with Noise (DBSCAN) and Related Algorithms. *Journal of Statistical Software*, 91(1), 1–30.

Hemmer, M., 2024. Algebraic Foundations. In CGAL User and Reference Manual. CGAL Editorial Board, 5.6.1 edition.

Hou, J., Luo, C., Qin, F., Shao, Y., Chen, X., 2023. FuS-GCN: Efficient B-rep based graph convolutional networks for 3D-CAD model classification and retrieval. *Advanced Engineering Informatics*, volume 56.

Jiang, T., Wang, Y., Zhang, Z., Liu, S., Dai, L., Yang, Y., Jin, X., Zeng, W., 2023. Extracting 3-D Structural Lines of Building From ALS Point Clouds Using Graph Neural Network Embedded With Corner Information. *IEEE Transactions on Geoscience and Remote Sensing*, vol. 61, pp. 1-28.

Kang, T., 2023. Scan to BIM Mapping Process Description for Building Representation in 3D GIS. *Appl. Sci.*, 13(17), 9986.

Khoshelham, K., Tran, H., Acharya, D., Díaz Vilariño, L., Kang, Z., Dalyot, S., 2020. The ISPRS benchmark on indoor modelling – preliminary results. *Int. Arch. Phot. Remote Sens. Spatial Inf. Sci.*, XLIII-B5-2020, 207–211.

Lee, Y.C., Ma, J.W. and Leite, F., 2023. A parametric approach towards semi-automated 3d as-built modeling. *Journal of Information Technology in Construction*, 28.

Liu, G., Wei, S., Zhong, S., Huang, S., Zhong, R., 2022. Reconstruction of Indoor Navigation Elements for Point Cloud of Buildings with Occlusions and Openings by Wall Segment Restoration from Indoor Context Labeling. *Remote Sensing*, 14(17):4275.

Maset, E., Magri, L., Fusiello, A., 2019. Improving automatic reconstruction of interior walls from point cloud data. *Int. Arch. Phot. Remote Sens. Spatial Inf. Sci.*, pp. 849-855.

Ning, X., Wang, M., Tang, J., Zhang, H., Wang, Y., 2021. Structural Wall Facade Reconstruction of Scanned Scene in Point Clouds. *Advances in Electrical & Computer Engineering*, 21(4), pp. 11-20.

Nguyen, T.D. and Adhikari, S., 2023. The role of BIM in integrating digital twin in building construction: A literature review. *Sustainability*, 15(13), 10462.

Ochmann, S., Vock, R., Klein, R., 2019. Automatic reconstruction of fully volumetric 3D building models from oriented point clouds, *ISPRS Journal of Photogrammetry and Remote Sensing*, Volume 151, 251-262.

Olimat, H., Liu, H., Abudayyeh, O., 2023. Enabling Technologies and Recent Advancements of Smart Facility Management. *Buildings*, 13(6), 1488.

Roman, O., Avena, M., Farella, E.M., Remondino, F. and Spanò, A., 2023a. A semi-automated approach to model architectural elements in SCAN-TO-BIM processes. *Int. Arch. Phot. Remote Sens. Spatial Inf. Sci.*, XLVIII-M-2-2023, 1345–1352.

Roman, O., Farella, E.M., Rigon, S., Remondino, F., Ricciuti, S. and Viesi, D., 2023b. From 3D surveying data to BIM and BEM: the INCUBE dataset. *Int. Arch. Phot. Remote Sens. Spatial Inf. Sci.,* XLVIII-1/W3-2023, 175–182.

Sampaio, A.Z., Gomes, A.M, 2021. BIM Interoperability Analyses in Structure Design. *CivilEng*, 2, 174-192.

Schmidt, J., Volland, V., Iwaszczuk, D. and Eichhorn, A., 2023. Detection of hidden edges and corners in slam-based indoor point clouds. *Int. Arch. Phot. Remote Sens. Spatial Inf. Sci.*, XLVIII-1/W1-2023, 443–449.

Tran, H., Khoshelham, K., 2020. Procedural Reconstruction of 3D Indoor Models from Lidar Data Using Reversible Jump Markov Chain Monte Carlo. *Remote Sensing*, 12, 838.

Wysocki, O., Xia, Y., Wysocki, M., Grilli, E., Hoegner, L., Cremers, D. and Stilla, U., 2023. Scan2LoD3: Reconstructing semantic 3D building models at LoD3 using ray casting and Bayesian networks. *Proc. CVPR*, pp. 6547-6557.

Xu Y., Stilla, U., 2021. Toward Building and Civil Infrastructure Reconstruction from Point Clouds: A Review on Data and Key Techniques. *IEEE Journal of Selected Topics in Applied Earth Observations and Remote Sensing*, vol. 14, pp. 2857-2885.

Yang, Y., Pan, Y., Zeng, F., Lin, Z. and Li, C., 2022. A gbXML reconstruction workflow and tool development to improve the geometric interoperability between BIM and BEM. *Buildings*, 12(2), 221.

Yang, F., Pan, Y., Zhang, F., Feng, F., Liu, Z., Zhang, J., Liu, Y. and Li, L., 2023. Geometry and Topology Reconstruction of BIM Wall Objects from Photogrammetric Meshes and Laser Point Clouds. *Remote Sensing*, 15(11), 2856.

Zhao, H., Jiang, L., Jia, J., Torr, P., Koltun, V., 2021. Point Transformer. *Proc. ICCV*, pp. 16259-16268.

Zhou, Y., Bao, T., Shu, X., Li, Y. and Li, Y., 2023. BIM and ontology-based knowledge management for dam safety monitoring. *Automation in Construction*, 145, 104649.